Journal of Earth Science, *Vol. 33*, *No. 6*, *p. 1535–1548*, *December 2022* *ISSN 1674-487X*
Printed in China
https://doi.org/10.1007/s12583-020-1376-9

Mineral Chemistry of Biotite and Its Petrogenesis Implications in ca. 2.5 Ga Wangjiazhuang Granitic Pluton, North China Craton

Junpeng Wang *[1, 2], **Kang Jiang**[1, 2], **Deng Xiao**[1, 2], **Fenfang Li**[1, 2], **Fupeng Li**[1, 2], **Xiaofeng Li**[3], **Song Jin**[3], **Guanghuo Tao**[3]

1. *School of Earth Sciences*, *Center for Global Tectonics*, *China University of Geosciences*, *Wuhan* 430074, *China*
2. *State Key Laboratory of Geological Processes and Mineral Resources*, *China University of Geosciences*, *Wuhan* 430078, *China*
3. *Hebei Institute of Geological Survey*, *Shijiazhuang* 050081, *China*

Junpeng Wang: https://orcid.org/0000-0003-2174-2428

ABSTRACT: The Wangjiazhuang granitic pluton is located in the central Zanhuang Domain, the central part of the North China Craton, which is mainly composed of biotite monzogranite with few mafic microgranular enclaves. Biotite is an important ferromagnesian mineral in most of the intermediate-felsic igneous rocks, and its mineral chemistry can record the properties of magma and the petrogenetic physicochemical conditions. In this study, we carried out a detailed petrographic study by electric probe microanalysis on biotite for the biotite monzogranite and mafic microgranular enclaves, to discuss the source, physicochemical conditions, and the magma mingling/mixing processes of the Wangjiazhuang granite. The results show significantly different chemical compositions from the biotite monzogranite and mafic microgranular enclaves. The crystallization of these biotite grains from the biotite monzogranite and mafic microgranular enclaves all occurred in low oxygen fugacity. The biotite grains in biotite monzogranite are rich in Fe, poor in Mg, which belong to siderophyllite. The ratios of [(Fe^{3+} + Fe^{2+})/(Fe^{3+} + Fe^{2+} + Mg^{2+})] are between 0.78 and 0.86. The average of FeO^T (total FeO)/MgO of biotite grains in biotite monzogranite is 9.02. The MF values [2 × Mg/(Fe^{2+} + Mg + Mn)] of biotite monzogranite are between 0.31 and 0.47, suggesting biotite monzogranite derived from crustal source rocks (metasedimentary rocks). The formation of granitic rocks including the Wangjiazhuang granite was related to the subduction event at ca. 2.5 Ga which resulted in the melting event, and then induced the early partial melting of TTGs and metasedimentary rocks. The biotite in mafic microgranular enclaves varies from siderophyllite to ferrobiotite, and MF values range from 0.63 to 1.06, suggesting that magma of mafic microgranular enclaves had experienced magma mixing/mingling in various degrees. Biotite monzogranite and parts of mafic microgranular enclaves have a similar crystallized condition, while other mafic microgranular enclaves are different from biotite monzogranite. The differences between biotite monzogranite and mafic microgranular enclaves may be a consequence of continuous interaction between granitic and mafic magmas.

KEY WORDS: biotite, mineral chemistry, crystallization, magma mixing, Wangjiazhuang granite, Zanhuang Massif, North China Craton.

0 INTRODUCTION

Emplacement of the granitic rocks (especially ca. 2.5 Ga) is developed within the whole North China Craton (NCC) in the late stage of the Neoarchean (Zhong et al., 2018; Han et al., 2014; Ma et al., 2013; Zhang et al., 2013; Nutman et al., 2011; Geng et al., 2010; Wilde et al., 2005). The Wangjiazhuang granitic pluton intrudes the Neoarchean Zanhuang tectonic mélange belt in the Central Orogenic Belt of the NCC (Jiang et al., 2020; Kusky et al., 2018; Wang J P et al., 2017a, b, c, 2015, 2013; Deng et al., 2013). The lithology of the Wangjiazhuang granitic pluton is relatively simple, mainly composed of biotite monzogranite and mafic microgranular enclaves (MMEs). Previous studies on the Wangjiazhuang granitic pluton put forward two main viewpoints about petrogenesis and the geodynamic mechanism by the whole-rock major and trace elements analysis: some researchers thought of it as being generated from remelting of old crust after accretion in a syn-subduction environment (Li and Zhai, 2019; Kusky et al., 2018; Wang J P et al., 2017b, 2015; Deng et al., 2014; Peng et al., 2013; Wang W et al., 2013; Nutman et al., 2011), whereas others thought of it as mantle sources (Kwan et al., 2016; Wu et al., 2014; Zhao and Zhai, 2013; Geng et al.,

*Corresponding author: wangjp@cug.edu.cn

Manuscript received October 28, 2020.
Manuscript accepted November 23, 2020.

Wang Junpeng, Jiang Kang, Xiao Deng, Li Fenfang, Li Fupeng, Li Xiaofeng, Jin Song, Tao Guanghuo, 2022. Mineral Chemistry of Biotite and Its Petrogenesis Implications in ca. 2.5 Ga Wangjiazhuang Granitic Pluton, North China Craton. *Journal of Earth Science*, 33(6): 1535–1548. https://doi.org/10.1007/s12583-020-1376-9. http://en.earth-science.net

2012; Zhao, 2009; Zhao et al., 1999). However, detailed mineral geochemical studies (e. g., biotite) play an important role in discussing the material source, physicochemical conditions and evolution history of magma crystallization.

The MMEs in granitoid are of great significance to explain the coexistence and mixing of two or more different types of magma during diagenesis, they play an important role in understanding the evolution of mafic magma in feldspar magma (Temizel et al., 2014; Weidendorfer et al., 2014; Liu et al., 2013; Yang and Jiang, 2013; Slaby and Martin, 2007; Zhang et al., 2007; Barbarin, 2005; Perugini et al., 2003). The study of magma mixing has become a hot topic in granite research recently. Mineral geochemistry data in magmatic rocks can provide direct evidence for physical and chemical conditions of magmatic consolidation and various geological processes (magma evolution processes such as separation crystallization, magma mixing, and magma consumption and replenishment) that occur in the magma chamber (Temizel et al., 2014; Speer, 1987). The chemical composition of minerals can reflect the physical and chemical parameters of mineral crystallization (pressure, temperature and oxygen fugacity, etc.), history of crystallization growth and source of magmatic materials.

Biotite is one of the most common melanocratic minerals which have a wide range of isomorphism of elements in their mineral chemical composition, such as Fe^{2+}-Mg-Mn, Si-Al-Fe-Ti and OH-F-Cl (Lü et al., 2003; Rieder et al., 1999; Sun and Yu, 1989). Metamorphic biotite has been used as a petrogenetic indicator. For example, biotite that coexists with certain key minerals is used as the garnet-biotite geothermometer (Wu, 2020; Wu and Zhao, 2007, 2006). Igneous biotite can also be used to provide valuable petrogenetic information, such as the chemical composition of biotite records the property of its host magma well, and its composition change can respond to the different geological environment and physicochemical conditions. In recent years, biotite has been applied to the research of magmatic mixing (Gao et al., 2016; Pignatelli et al., 2016). Therefore, the study of biotite is of important geological significance and has been widely used in the study of magmatic genesis (Zhao K D et al., 2019, 2005; Xu B et al., 2015; Zhao M et al., 2015; Zhu et al., 2014; Xu Y M et al., 2013; Dong et al., 2011; Jiang et al., 2008, 2006; Zhang et al., 2005; Stone, 2000; Peng, 1997; Abdel-Rahman, 1996, 1994; El Sheshtawi et al., 1993; Burkhard, 1991).

To further reveal the petrogenesis of Wangjiazhuang granite and MMEs, especially to reveal whether magmatic mixing occurred during the formation process of this granitoid, detailed petrographic and mineral chemical characteristics of biotite in Wangjiazhuang granitoid are studied. By comparing biotite in granite and MMEs of Wangjiazhuang granitoid and combining previous rock geochemistry data (zircon U-Pb dating, whole-rock major and trace elements analysis, Sr-Nd isotopic composition), the petrogenesis of Wangjiazhuang granitoid and its mixing process with mafic inclusion magma are further discussed in this study.

1 GEOLOGICAL BACKGROUND

The North China Craton (NCC) covers about 1.7 million square kilometers in northeastern China, Inner Mongolia, the Yellow Sea, and Korea. It is bounded to the south by the Qinling-Dabie Belt, the Central Asian Orogenic Belt to the north, the Qilian Orogen to the west, and the Jiao-Liao Belt to the east (Chen et al., 2021; Guo et al., 2021; Du et al., 2020; Duan et al., 2020; Ma et al., 2019; Kusky et al., 2018, 2016; Kusky and Li, 2003; Bai and Dai, 1998, 1996). It is one of the most intact paleo-continental cratons in China and even in the world (Fig. 1a). For recent decades, most researchers have generally divided the NCC into the Eastern Block (EB) and the Western Block (WB), separated by the intervening Central Orogenic Belt (Zhao et al., 2001; Kusky and Li, 2003), or several smaller microblocks (Zhai and Santosh, 2011; Li et al., 2010), which are separated by greenstone belts with different ages (2.5, 2.6–2.7 Ga). The Zanhuang Block is located in the easternmost margin of the central south section of the orogenic belt in the central part of the North China Craton (Fig. 1b), and it is one of the key areas to study and analyze the collision orogenic effect of the eastern and western continental blocks of the North China Craton. Trap et al. (2011, 2009a, b) divided the Zanhuang Block into three tectonic geological units: the western Zanhuang Domain, the eastern Zanhuang Domain and the central Zanhuang Domain. The Wangjiazhuang granite (Fig. 1c) is located in the southwest corner of Hebei Province, at the junction of the central and eastern Zanhuang Domain, which has an exposed area of about 12 km^2, with an irregular annular body.

The lithology of Wangjiazhuang granite is relatively simple, mainly composed of biotite monzogranite (Fig. 2). Previous studies on the Wangjiazhuang granite have been underway for many years. Wang et al. (2015) carried out the petrochemistry study of the Wangjiazhuang granite, including zircon U-Pb dating, whole-rock major and trace elements analysis and Sr-Nd isotopic composition, considered a typical affinity of A-type granite of the Wangjiazhuang granite, with high Si, K and Rb/Sr ratios (1.8–3.21, average 2.54), low Mg and Cr content. It indicated that the Wangjiazhuang granite did not crystallize directly from the mantle source, but underwent a certain degree of crustal mixing.

2 SAMPLE DESCRIPTION

Fresh granite and MMEs with different color index were sampled from the edge to the core of the Wangjiazhuang granite (Fig. 2). The Wangjiazhuang granite has pink to reddish hues, which shows the gneissose and massive structure (Fig. 3a). The orientation of biotite minerals can be observed from samples at the edge of the granitoid. The main minerals include feldspar (55%–60%), quartz (25%–30%), biotite (5%–10%), muscovite (<5%) and minor magnetite, apatite and zircon. Feldspar grains are mostly microcline and are variably sericitized (Fig. 3d). The MMEs exist in the whole Wangjiazhuang granite, mainly showing irregular- or spindle-shaped, with different sizes (Figs. 3b and 3c). The smaller MMEs are 5–8 cm in diameter whereas some MMEs reach up to 100 cm in diameter. There are clear or transitional boundary between the different MMEs and the granite (Figs. 3b and 3c). The color index of MMEs is different, and a complete series can be formed according to the color index. The MMEs are generally darker than granite and also show the massive structure. Some have porphyritic-like texture while others show micrograined or

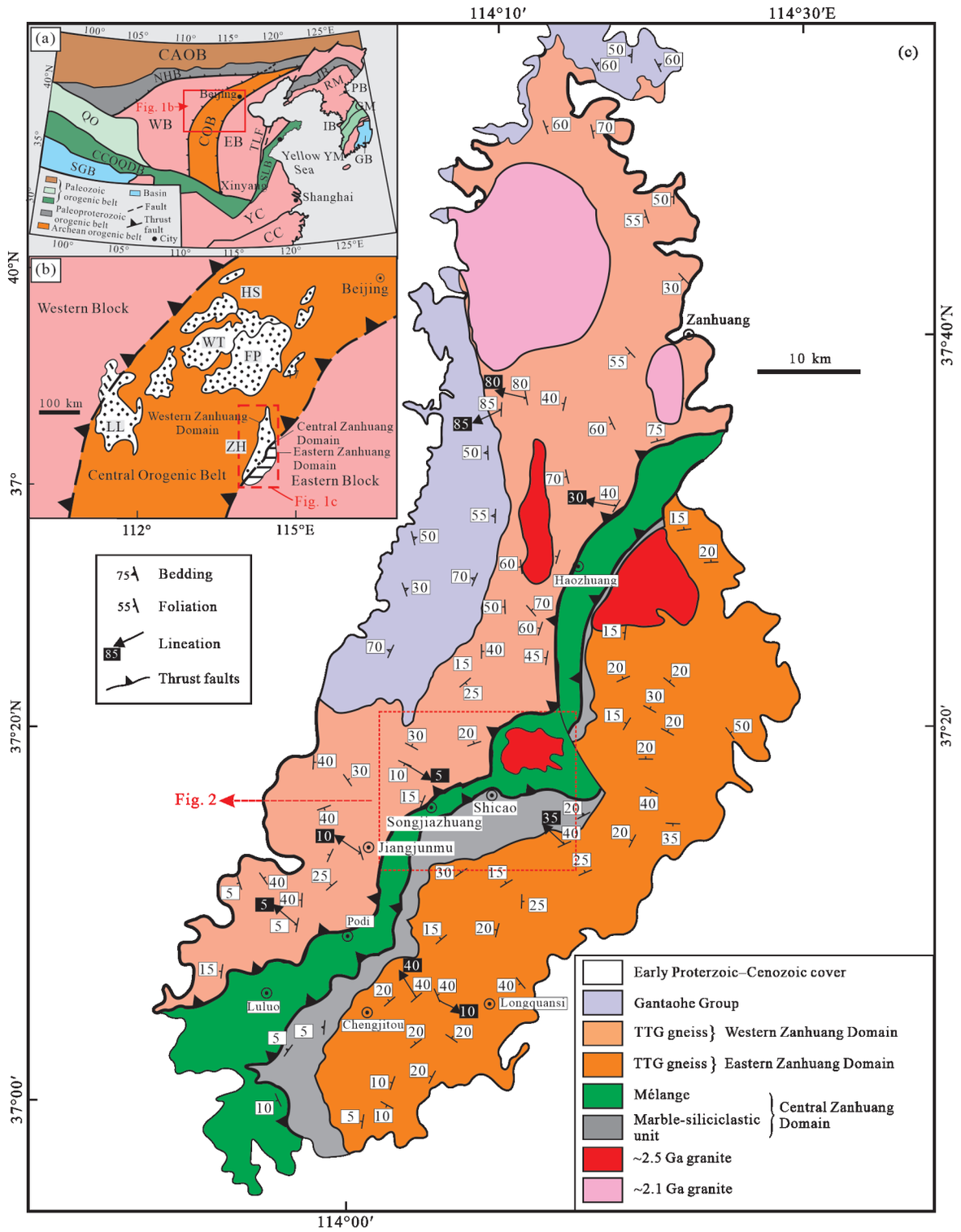

Figure 1. (a) Tectonic subdivision of the North China Craton (NCC) including the Western Block (WB), the Eastern Block (EB) and the Central Orogenic Belt (COB); QO. Qilian Orogen; CCOQDB. Central China Orogen Qinling-Dabie Belt; SGB. Songpan-Ganzi Basin; NHB. North Hebei Orogen; JB. Jiaoliao Belt; SLB. Sulu Belt; TLF. Tanlu fault; RM. Ramgnim massif; PB. Pyeongnam Basin; GM. Gyeonggi massif; IB. Imjingang Belt; YM. Yeongnam massif; GB. Gyeongsang Basin; YC. Yangtze Craton; CC. Cathaysia Craton. (b) Geological map of the central part of the North China Craton (NCC) showing different massif within the Central Orogenic Belt, and the western, central, and eastern Zanhuang domains of the Zanhuang massif; HS. Hengshan massif; WT. Wutaishan Massif; FP. Fuping massif; LL. Lüliangshan massif; ZH. Zanhuang massif; (c) geological map of the Zanhuang massif, the western Zanhuang Domain mainly consists of circa 2.5–2.6 Ga TTG gneiss. Maps modified after Trap et al. (2009a) and Wang et al. (2015).

equigranular texture. The main minerals include feldspar (40%–45%), quartz (30%–35%), biotite (20%–25%), and minor magnetite, apatite and zircon (Figs. 3e and 3f). Feldspar grains are mostly K-feldspar and albite.

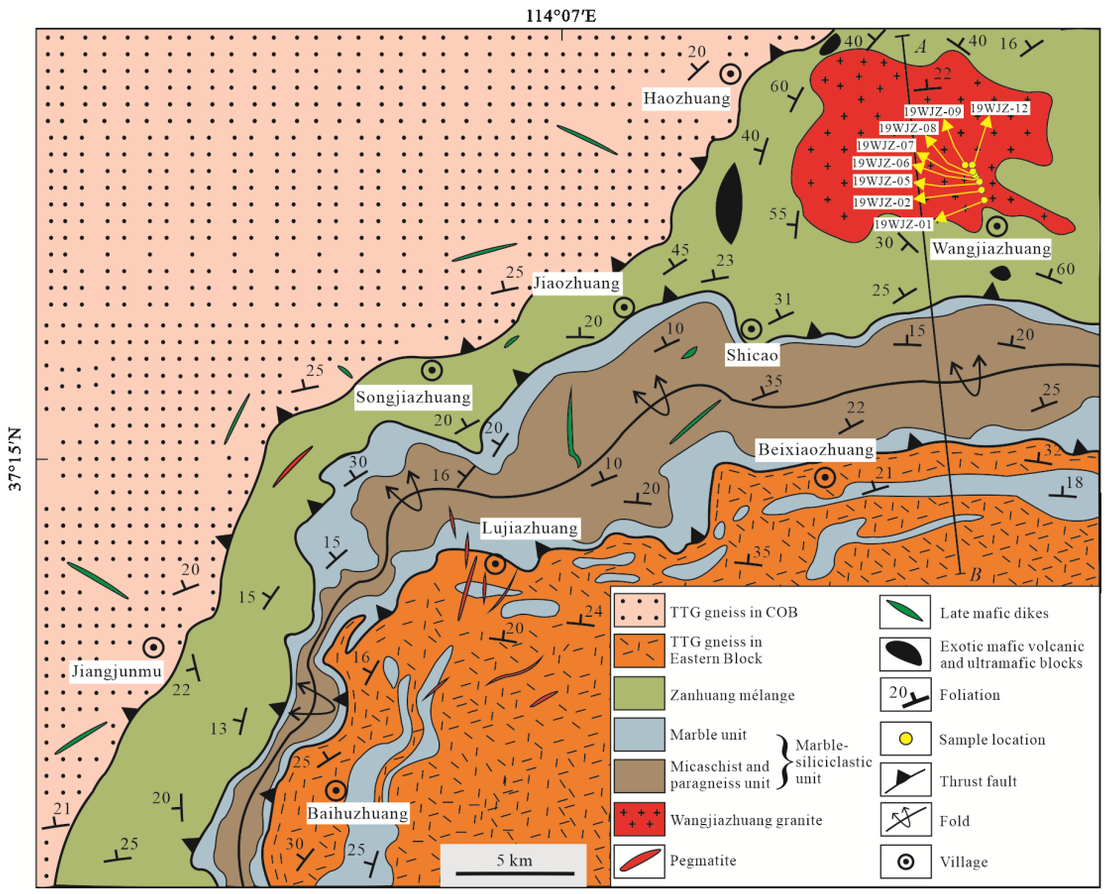

Figure 2. Geological map of the study area showing sample locations and the different units, including the TTG gneisses of the western Zanhuang Domain and the Eastern Block, the Neoarchean mélange belt, marble unit and mica schist and paragneiss unit of the marble-siliciclastic unit; the mélange is intruded by the Wangjiazhuang granitic pluton with surrounding schist, marble, quartzite and volcanic rocks and cross-cut by undeformed pegmatites (modified after Wang J P et al., 2013).

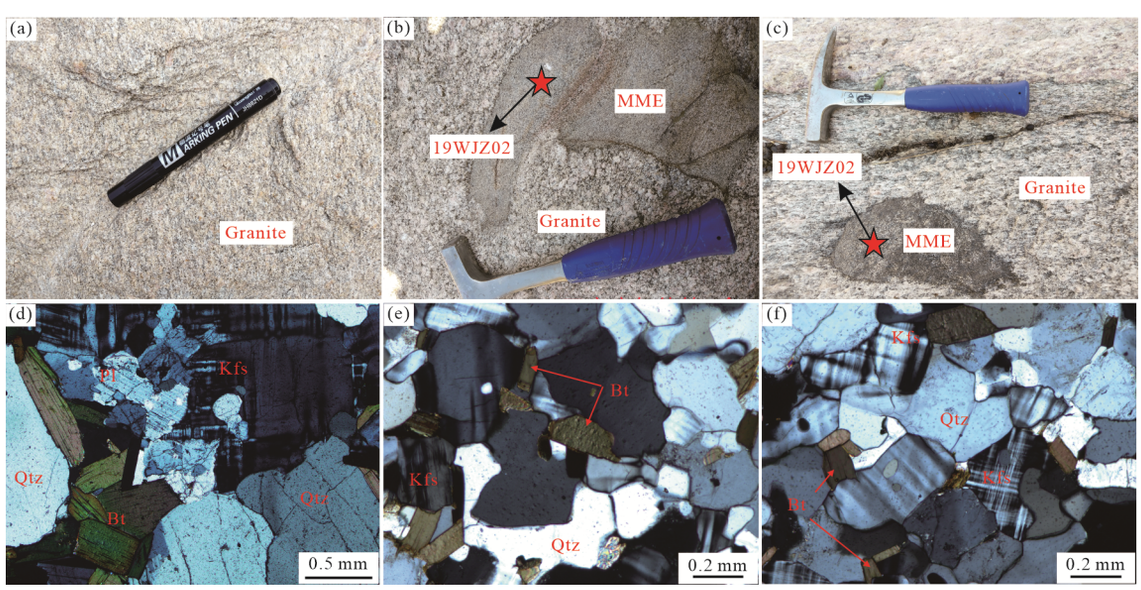

Figure 3. Field photographs and microphotographs of the Wangjiazhuang granite and MMEs. (a) The Wangjiahzuang granite in the field; (b) and (c) the MMEs in the Wangjiazhaung granite; (d) granite containing K-feldspar (Kfs), plagioclase (Pl), quartz (Qtz) and biotite (Bt); (e) and (f) the MME containing K-feldspar (Kfs), quartz (Qtz) and biotite (Bt).

3 ANALYTICAL METHODS AND RESULTS

Mineral analyses were performed using a JEOL JXA-8230 electron probe microanalyzer (EPMA) with four wavelength-dispersive spectrometers (WDS) at the Center for Global Tec-

tonics, School of Earth Sciences, China University of Geosciences (Wuhan). The operating conditions were described in Wang et al. (2019) and Ning et al. (2019) in detail. A 15 kV accelerating voltage, 20 nA probe current, and a one-micron beam diameter had been used. Dwell times were 10 s on element peaks and half that on background locations adjacent to peaks. Raw X-ray intensities were corrected using a ZAF (atomic number, absorption, fluorescence) correction procedure. A series of natural and synthetic SPI standards were utilized and changed based on analyses of the minerals. The following standards were used: sanidine (K), pyrope garnet (Fe, Al), diopside (Ca, Mg), jadeite (Na), rhodonite (Mn), olivine (Si), rutile (Ti) and apatite (P). The structural formula of biotite was calculated based on 22 oxygens, and the Fe^{2+} and Fe^{3+} contents in biotite were calculated by the method of Lin and Peng (1994). The calculation results are shown in Table 1.

Whole-rock major and trace element geochemical analysis were carried out at the State Key Laboratory of Geological Processes and Mineral Resources in China University of Geoscience (Wuhan). Eight MMEs samples were crushed to ~200 μm powder respectively before the geochemical analysis. Major element contents were measured by Shimadzu scanning X-ray fluorescence spectrometry (XRF). The analytical precision and accuracy are >4%. Measurement procedures and data quality assessment are monitored by repeated analysis of the USGS standard AGV-2 and Chinese National standards GSR-3 and GRS-7. Specific analytical conditions and processes are presented in Ma et al. (2012). Trace element contents were determined using an Agilent 7500a inductively-coupled plasma-mass spectrometer (ICP-MS). International standard samples of BHVO-2, AGV-2 and RGM-2 were used in the analysis. Details of sample processing and analytical procedures are given in Govindaraju (1994) and Liu et al. (2008).

Table 1 Electron microprobe analysis of the biotite from biotite monzogranite and MME (wt.%)

	Biotite monzogranite (n = 52)			MMEs (n = 200)		
	Min	Max	Mean	Min	Max	Mean
SiO_2	34.41	35.71	35.07	34.27	38.64	35.83
TiO_2	2.35	3.3	2.73	0.34	3.62	2.01
Al_2O_3	15.43	17.05	16.07	13.01	17.42	16.03
FeO^T	27.33	29.02	27.92	20.22	28.08	24.08
MnO	0.16	0.33	0.24	0.2	0.67	0.4
MgO	2.52	4.26	3.14	3.51	9.83	6.38
CaO	0	0.16	0.01	0	11.29	0.12
Na_2O	0.01	0.5	0.11	0	1.51	0.06
K_2O	9.17	10.32	10.04	2.23	10.3	9.86
F	0.41	1.6	0.94	0.57	2.8	1.71
O = F	0.24	0.93	0.54	0.33	1.62	0.99
Total	95.37	96.38	95.87	94.56	96.69	95.77
FeO^T/MgO	6.42	10.89	9.02	2.15	7.6	4.35
Si	5.66	5.39	5.56	5.41	5.86	5.60
Ti	0.29	0.37	0.33	0.04	0.43	0.24
Al^{IV}	2.34	2.61	2.44	2.14	2.59	2.40
Fe^{2+}	3.26	3.34	3.27	2.25	3.37	2.78
Fe^{3+}	0.50	0.32	0.43	0.23	0.48	0.38
Mn	0.02	0.04	0.03	0.03	0.09	0.05
Mg	0.62	0.96	0.74	0.82	2.28	1.48
Ca	0.00	0.03	0.00	0.00	1.84	0.02
Na	0.00	0.15	0.03	0.00	0.44	0.02
K	1.92	1.99	2.03	0.43	2.07	1.97
MF	0.31	0.47	0.37	0.42	0.95	0.67
$(Fe^{2+} + Fe^{3+})/(Fe^{2+} + Fe^{3+} + Mg)$	0.78	0.86	0.83	0.55	0.81	0.69

Results of the EPMA are shown in Table 1, and the trend diagram of biotite composition is shown in Fig. 4, which indicates that the Wangjiazhuang granite is characterized by enrichment in Fe, Ti, Al content and depletion in Mg content (Figs. 4b, 4c and 4e). The FeO^T (total iron, the same below) fraction of biotite in granite is 27.33 wt.%–29.02 wt.%, the mass fraction of MgO is 2.52 wt.%–4.26 wt.%, and the iron coefficient $[(Fe^{3+} + Fe^{2+})/(Fe^{3+} + Fe^{2+} + Mg^{2+})]$ is 0.65–0.70. The chemical composition of biotite from MMEs is obviously different from that of the former, showing that the FeO^T value is 20.22 wt.%–28.08 wt.%, MgO is 3.51 wt.%–9.83 wt.%, the iron coefficient $[(Fe^{3+} + Fe^{2+})/(Fe^{3+} + Fe^{2+} + Mg)]$ is 0.55–0.81. The values of Si, Al, Mg and F vs. $[(Fe^{3+} + Fe^{2+})/(Fe^{3+} + Fe^{2+} + Mg)]$ show significant negative correlations while others show positive correlations or irrelevance (Figs. 4a – 4f). Compared with biotite in granite, Mg and Fe content of biotite in MMEs varies widely. The composition of biotite in some MMEs is similar to that in granite, while some are relatively rich in Mg and poor in Fe. During the transition from MMEs to granite, the mean value of MF $[2 \times Mg/(Fe^{2+} + Mg + Mn)]$ decreases continuously from 0.67 to 0.37.

Eight samples of MMEs have been analyzed for major and trace elements. The major oxides described below are recalculated to 100% on a volatile-free basis. The results and related parameters are shown in Table 2. The MMEs have a relatively narrow range of geochemical compositions, with SiO_2 content between 67.28 wt.% and 73.64 wt.%, high Al_2O_3 between 12.86 wt.% and 15.57 wt.%, MgO between 0.30 wt.% and 1.79 wt.%, Fe_2O_3 between 2.36 wt.% and 5.65 wt.%, and CaO between 0.86 wt.% and 3.56 wt.%. As shown in Table 2, these rocks are relatively rich in alkalis with K_2O of 1.02 wt.% – 5.79 wt.%, Na_2O of 2.72 wt.%–5.18 wt.%, and total alkalis ($K_2O + Na_2O$) of 3.74 wt.% – 10.97 wt.%, whereas low TiO_2 content of 0.22 wt.%–0.43 wt.%. The values of $Mg^{\#}$ range from 19 to 39. The MMEs have a large variation and enrichment in trace elements with Ga of 20.8 ppm–29 ppm, Rb of 132.5 ppm–360 ppm, Zr of 107 ppm–472 ppm, Nb of 6.9 ppm–25.1 ppm, Y of 7.9 ppm–49.7 ppm (Table 2). The total REEs content of MMEs are high (Table 2), and show wide variations (ΣREE = 70.8 ppm–938.2 ppm, average value = 272.1 ppm) with very strong negative Eu anomalies (Eu/Eu* = 0.2–1.13). The MMEs are highly enriched in LREEs ($(La/Sm)_N$ = 3.36–5.70; $(La/Yb)_N$ = 9.25–46.03) and have relatively flat HREE ($(Gd/Yb)_N$ = 1.52–4.7) patterns.

The biotite in the granite can be formed by metamorphic or igneous origin. Ma et al. (1994) proposed a discrimination method by the chemical composition of the biotite. The biotite

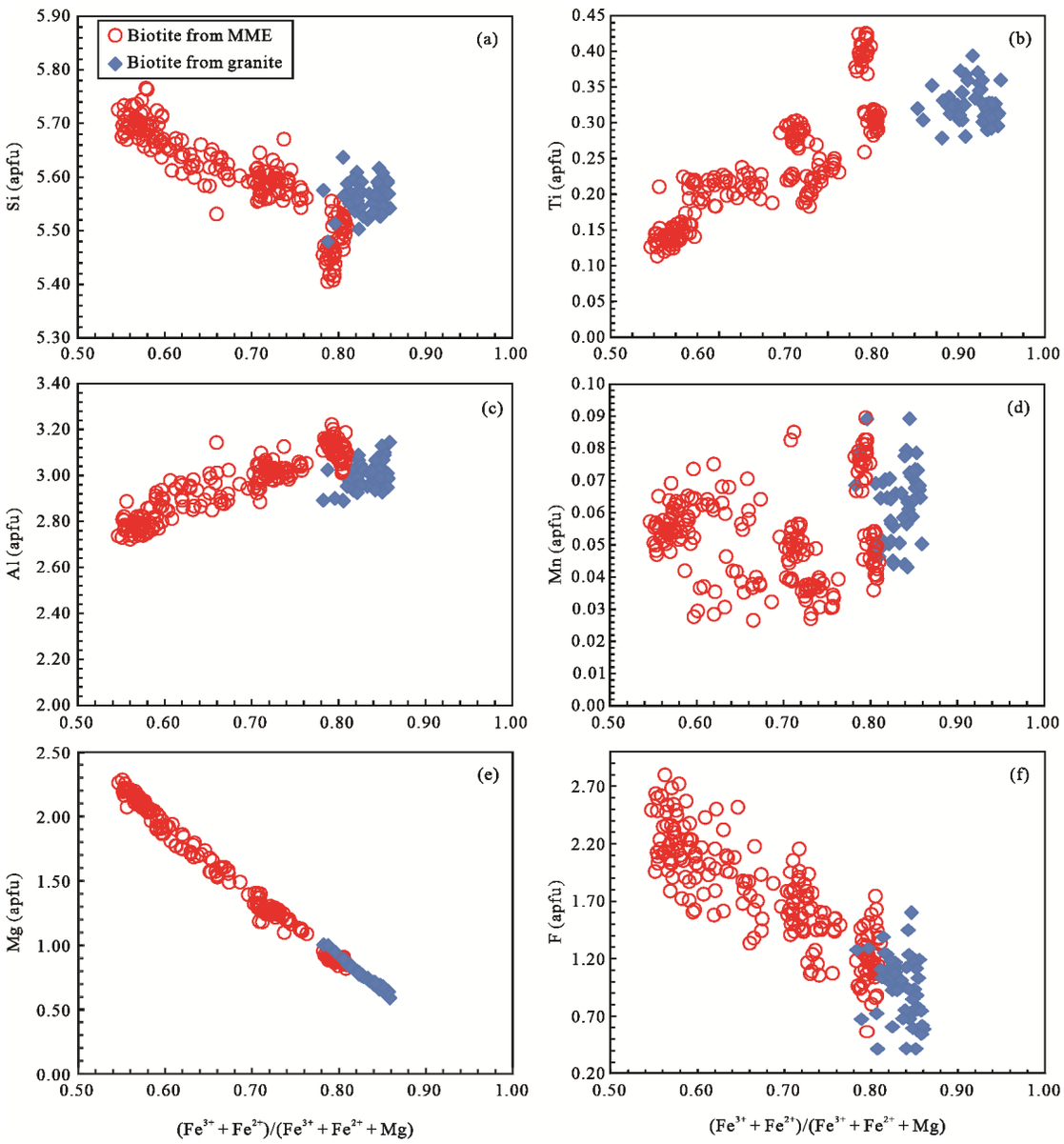

Figure 4. Composition variations of biotites in biotite monzogranite and MMEs from Wangjiazhuang pluton.

formed by retrograde metamorphism with the Ti content (atoms per formula unit, apfu) lower than 0.2 or formed by prograde metamorphism with the variable Ti content (apfu) and Mg/(Mg + Fe) content are higher than 0.55. The biotite formed by igneous origin with higher Ti content (0.2–0.55, apfu) and moderate Mg/(Mg + Fe) content (0.3–0.55, apfu). The biotite grains from MMEs are characterized by Ti values of 0.17–0.43 (0.28 on average, apfu) and Mg/(Mg + Fe) values of 0.19–0.45 (0.32 on average, apfu) (Figs. 4b and 4e). The biotite grains from granite are characterized by Ti values of 0.27–0.39 (0.33 on average, apfu) and Mg/(Mg + Fe) values of 0.14–0.22 (0.16 on average, apfu) (Figs. 4b and 4e). Combining with mostly biotite grains from MMEs and granite are euhedral, we infer the biotite grains are mostly igneous origin.

The TiO_2 and Al_2O_3 contents of biotite in granite show narrow variations, the range of TiO_2 content is 2.35 wt.% to 3.30 wt.%, and Al_2O_3 content is 15.43 wt.% to 17.05 wt.%. However, the range of Al and Ti content of biotite in MMEs is relatively wide, which is related to the mixing degree of enclave magma and host magma and the change of crystallization environment of biotite (Temizel et al., 2014).

In the Mg-(Al^{VI} + Fe^{3+} + Ti)-(Fe^{2+} + Mn) biotite classification diagram (Fig. 5), the biotite in granite falls into the field of siderophyllite, and the biotite in MMEs is widely distributed, including ferro-biotite and siderophyllite.

4 DISCUSSION

4.1 Petrogenesis

The composition characteristics of biotite in magmatite well recorded the physicochemical information of host magma (Abdel-Rahman, 1996, 1994). Using biotite coexisting with magnetite and potash feldspar, Wones and Eugster (1965) experimentally studied the contents of Fe^{3+}, Fe^{2+} and Mg in biotite, concluding that these three factors could recover the oxygen fugacity during the crystallization process of mica. According to the microscope observation and the composition of biotite

Table 2 Chemical composition for mafic microgranular enclaves and their host rocks from Wangjiazhuang pluton

Lithology	MMEs							
Reference	This study							
Sample	19WJZ01	19WJZ02	19WJZ05	19WJZ06	19WJZ07	19WJZ08	19WJZ09	19WJZ12
GPS	37°17′55″N 114°13′25″E	37°17′58″N 114°13'24″E	37°18′3″N 114°13'29″E	37°18′9″N 114°13'20″E	37°18'12″N 114°13'21″E	37°18'13″N 114°13'30″E	37°18′16″N 114°13'26″E	37°18′20″N 114°13'31″E
SiO_2	67.28	72.48	68.19	67.73	68.68	73.64	73.19	70.04
TiO_2	0.43	0.31	0.41	0.41	0.35	0.22	0.25	0.35
Al_2O_3	15.57	13	12.86	13.06	14.22	13.53	13.1	12.92
Fe_2O_3	4.25	3	5.42	5.64	5.12	2.41	2.36	5.65
MnO	0.06	0.04	0.12	0.1	0.06	0.05	0.05	0.08
MgO	0.96	0.35	1.77	1.79	1.11	0.71	0.3	0.91
CaO	1.85	1.09	3.56	3.43	1.76	2	0.86	1.96
Na_2O	4.94	2.72	4.03	4.1	4.17	5.18	2.92	4.26
K_2O	3.35	5.79	1.78	2.05	3.25	1.02	5.77	1.98
P_2O_5	0.14	0.05	0.12	0.13	0.1	0.05	0.05	0.1
LOI	0.78	0.84	1.22	1.36	0.65	0.69	0.75	1.03
Total	99.61	99.67	99.48	99.8	99.47	99.5	99.6	99.28
La	57.2	220	15.4	15.6	15.5	20.5	135	21.5
Ce	116	440	28.7	29.5	29.4	34.7	287	32.7
Pr	11.8	51	3.44	3.67	3.9	4.44	31	5.2
Nd	40	158.5	14	13.3	13.9	14.9	99.8	19.3
Sm	6.48	26.2	2.25	2.28	2.26	2.66	16.05	4.13
Eu	1.12	1.37	0.69	0.83	0.39	0.49	1.2	0.42
Gd	4.53	16.8	2.09	2.23	1.92	2.5	11.25	4.06
Tb	0.62	2.25	0.36	0.32	0.27	0.35	1.37	0.63
Dy	3.52	10.9	2.05	2.03	1.43	1.99	6.89	3.36
Ho	0.66	2.03	0.41	0.45	0.27	0.42	1.17	0.62
Er	1.87	4.6	1.18	1.21	0.73	1.09	2.65	1.52
Tm	0.27	0.58	0.17	0.18	0.1	0.16	0.34	0.21
Yb	1.93	3.43	1.09	1.21	0.61	1.01	1.98	1.17
Lu	0.3	0.54	0.15	0.17	0.09	0.16	0.32	0.15
Ba	509	802	117.5	139	277	91.3	804	159.5
Nb	25.1	20.4	6.9	7.5	15	7.7	15.6	20.1
Rb	360	326	225	272	292	132.5	258	294
Sr	235	126	124	121.5	138	149.5	122.5	103
Th	12.9	42.9	2.09	2.08	1.96	4.01	30.2	3.6
Ti	0.26	0.19	0.25	0.25	0.2	0.13	0.16	0.22
U	4.35	3.09	0.7	0.69	0.5	1.04	2.21	0.64
Y	19.1	49.7	11.1	12	7.9	10.6	24.6	16.7
Zr	195	472	128	123	122	107	334	125
Hf	4.8	13.8	2.7	3.2	3.1	3.2	9.9	3.5
Eu/Eu*	0.63	0.2	0.97	1.13	0.57	0.58	0.27	0.31
La/Sm	5.7	5.42	4.42	4.42	4.43	4.98	5.43	3.36
La/Yb	21.27	46.03	10.14	9.25	18.23	14.57	48.93	13.19
Gd/Yb	1.94	4.05	1.59	1.52	2.6	2.05	4.7	2.87
Age (Ma)								
$\varepsilon_{Nd}(t)$								

Table 2 Continued

Lithology	Biotite monzogranite						
Reference	Wang et al. (2015)						
Sample	13XT-17-1	13XT-19-1	13XT-22-1	13XTA-20	13XTA-21	13XTA-22	13XTA-23
GPS	37°19'36"N 114°11'30"E	37°19'37"N 114°11'19"E	37°18'1"N 114°13'30"E	37°17'55"N 114°13'29"E	37°17'57"N 114°13'30"E	37°17'59"N 114°13'30"E	37°17'59"N 114°13'30"E
SiO_2	74.61	74.23	73.91	72.87	72.56	72.8	73.29
TiO_2	0.21	0.25	0.23	0.25	0.23	0.2	0.26
Al_2O_3	13.57	13.22	13.49	13.24	13.62	13.31	13.21
Fe_2O_3	1.84	2.25	2.28	2.33	2.38	2.02	2.6
MnO	0.03	0.04	0.03	0.03	0.04	0.03	0.05
MgO	0.39	0.37	0.29	0.5	0.29	0.29	0.41
CaO	1.12	1.07	1.16	0.53	1.04	1	1.15
Na_2O	3.5	3.08	3.3	2.86	3.05	3.15	2.97
K_2O	5.29	5.83	5.6	6.03	5.87	5.57	5.37
P_2O_5	0.06	0.06	0.05	0.06	0.05	0.04	0.06
LOI	0.41	0.59	0.45	0.71	0.68	0.76	0.9
Total	101	101	100.8	99.41	99.81	99.17	100.3
La	60.1	90.5	105	87.7	109	95.2	133
Ce	121	188	217	190	213	211	271
Pr	13.1	20.5	23.8	20.5	24.4	21.4	29.8
Nd	45.6	72.3	83	70.7	85.6	75.8	102.4
Sm	8.78	13.1	14.3	11.6	14.8	13	17.4
Eu	0.71	1.02	1.13	0.98	1.26	1.05	1.25
Gd	8.13	10.8	11.4	7.13	10.9	9.19	12.2
Tb	1.43	1.59	1.62	1.04	1.65	1.34	1.76
Dy	9.3	8.87	8.75	5.32	8.67	7.14	8.95
Ho	1.88	1.63	1.65	1.03	1.58	1.27	1.54
Er	5.54	4.63	4.57	2.82	4.54	3.51	3.79
Tm	0.83	0.62	0.65	0.46	0.66	0.5	0.51
Yb	5.09	4.03	3.99	2.8	4.14	3.13	3.04
Lu	0.6	0.56	0.56	0.5	0.66	0.53	0.47
Ba	453	533	543	562	555	577	618
Nb	20.9	24.7	22	19.8	24.3	17.4	15.5
Rb	294	282	263	292	269	291	232
Sr	109	105	116	91.1	116	105	129
Th	23.2	29.3	27.1	30.4	28.7	27.8	30.8
Ti	1.4	1.36	1.24	1.33	1.27	1.35	1.06
U	3.72	3.36	4.29	2.08	2.2	2.53	2.71
Y	56.8	47.9	48.6	30.9	47.6	35.5	40.8
Zr	206	272	267	306	302	274	355
Hf	6.56	8.29	8.13	8.8	9.23	8.34	10.6
Eu/Eu*	7.21	6.84	6.61	5.84	6.27	6.08	6.21
La/Sm	4.42	4.46	4.74	4.88	4.75	4.73	4.93
La/Yb	8.47	16.11	18.88	22.47	18.89	21.82	31.38
Gd/Yb	1.32	2.22	2.36	2.11	2.18	2.43	3.32
Age (Ma)	2 517 ± 20	2 506 ± 9.8	2 513 ± 13				
$\varepsilon_{Nd}(t)$	0.12	0.76	1.13				

Major elements, wt.%; trace elements, ppm; LOI. loss on ignition.

grains by EPMA, biotite in this study conforms to the conditions of the described estimation method above. In the triangle diagram of Fe^{3+}-Fe^{2+}-Mg (Fig. 6), the point for the composition of biotite grains from granite and MMEs are both located near the Ni-NiO buffer line, indicating that all biotite grains were crystallized under the condition with low oxygen fugacity.

The variation range of MF values of biotite in granite and MMEs is 0.31–0.47 and 0.42–0.95, respectively. According to the summary of the genetic types of granite (Xie and Zhang, 1987), the MF values of biotite in granite from this study are between 0.31 and 0.95, which are typical characteristics of ferrobiotite, indicating the granite is crust-derived. Zhou (1988) used FeO^T/ (FeO^T + MgO)-MgO diagram to distinguish mica from three different material source. All the data from MMEs and granite show a very obvious negative correlation, respectively. The Wangjiazhuang granite shows the typical characteristics of crust-derived granite (Fig. 7). The biotite in small parts of MMEs falls into the crust-mantle mixing area while the other biotite falls into the crust source area, indicating a continuous change in the crystallization of the MMEs, and parts of MMEs with higher MgO values may have preserved the compositions closer to the original source of material. Since the final evolution trend result is close to the granite, we speculate that the biotite monzogranite is the final result of magma mixing (Fig. 7).

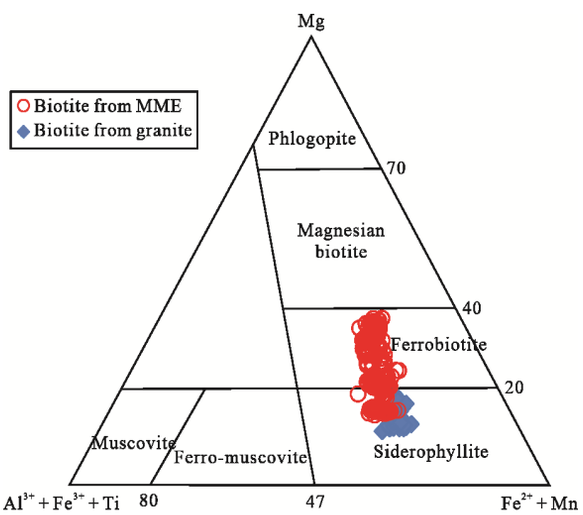

Figure 5. Classification diagram for biotites in biotite monzogranite and MMEs from Wangjiazhuang (after Foster, 1960).

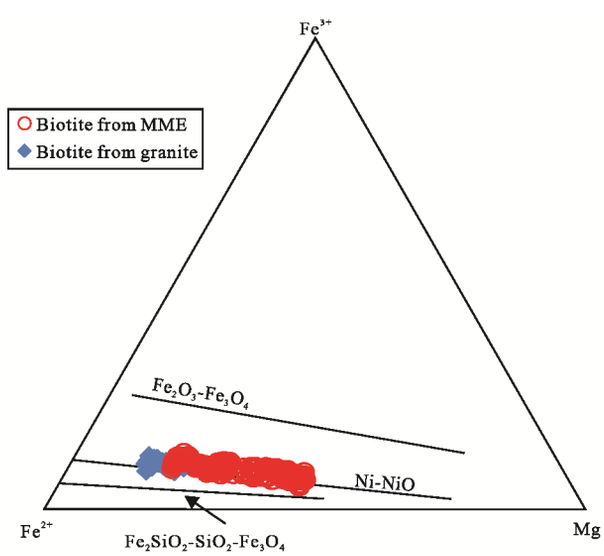

Figure 6. Fe^{3+}-Fe^{2+}-Mg ternary diagram for biotite monzogranite and MMEs from Wangjiazhuang pluton (after Wones and Eugster, 1965).

Abdel-Rahman (1994) systematically studied the biotite composition in orogenic and anorogenic rocks, and proposed a discriminant diagram for the use of biotite composition to distinguish the tectonic environment (Fig. 8a), and pointed out that in the calc-alkaline orogenic suites (I-type granites, field C), biotite is moderately enriched in Mg with an average FeO^T/MgO ratio of 1.76; biotite in the peraluminous (including S-type granites) series (field P) are siderophyllitic in composition and have an average FeO^T/MgO ratio of 3.48; biotites in anorogenic alkaline suites (field A) are mostly iron-rich, siliceous biotites (near annite), with an average FeO^T/MgO ratio of 7.04 (Abdel-Rahman, 1994). However, Shabani et al. (2003) studied the biotite geochemical characteristics of the Paleozoic granites of different origins of Canadian Appalachians, and believed that the biotite composition can reflect the original characteristics of the host magma, which cannot be readily used for tectonomagmatic characterization of these rocks without the aid of other types of data. The combined use of multiple discriminant diagrams with other relevant geological evidence may provide us with more accurate information. Here we chose two discrimination diagrams from Abdel-Rahman (1994) and Shabani et al. (2003) to discuss the tectonic setting of MMEs and granite. On the Fe/(Fe + Mg) vs. Al diagram, biotite grains from granite are characterized by enriched Al and Fe/(Fe + Mg) content and plotted in the I-SCR (strongly contaminated and reduced I-type) granites field; biotite grains from MMEs are characterized by variable Al and Fe/(Fe + Mg) content and plotted in the I-SCR or continental arc field (Fig. 8b). On the FeO^T-MgO-Al_2O_3 diagram, biotite grains from granite are plotted in the fields A or P while biotite grains from MMEs plot in the fields P or C (Fig. 8a). We can clearly see that there is a similar evolutionary trend of MMEs from two diagrams that tectonic setting has transitioned from an active environ-

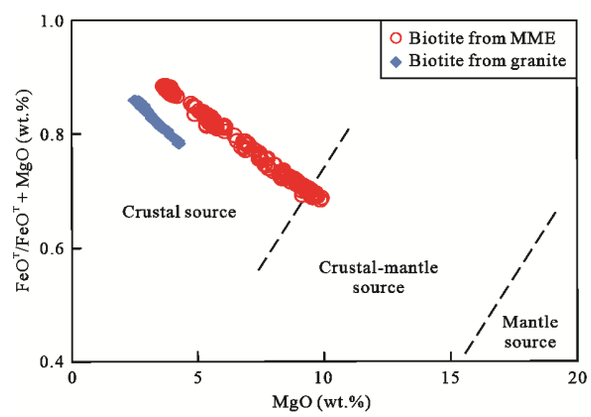

Figure 7. FeO^T/(FeO^T + MgO)-MgO diagram on material sources of biotites in biotite monzogranite and MMEs from Wangjiazhuang pluton (after Zhou, 1988).

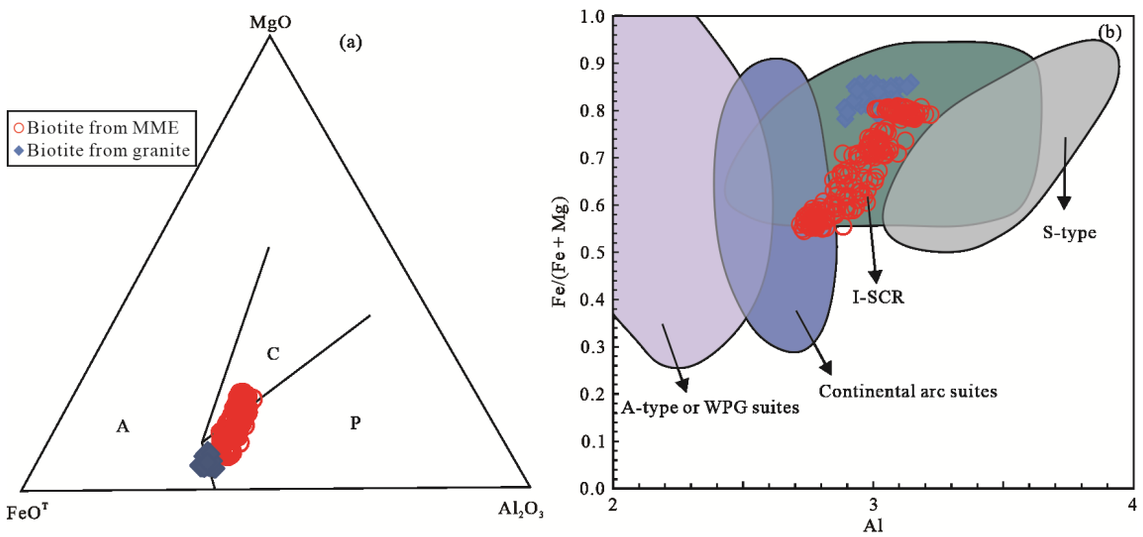

Figure 8. (a), (b) Classification diagrams of structural setting for biotites in MMEs and biotite monzogranite (after Abdel-Rahman, 1994 and Shabani et al., 2003); I-SCR. strongly contaminated and reduced I-type granite; field A. alkaline (mostly anorogenic extensional-related) suites including A-type granites; field C. calc-alkaline (mostly orogenic subduction-related) suites including I-type granites; field P. peraluminous rocks including collisional and S-type granites).

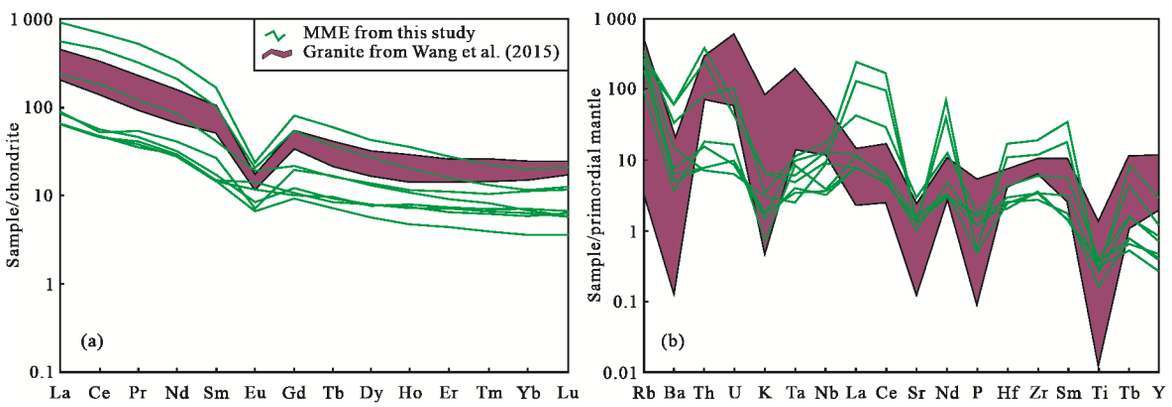

Figure 9. (a) Chondrite-normalized REE distribution patterns and (b) primitive mantle-normalized spidergrams of the MMEs (normalization values from McDonough and Sun, 1995).

ment (continental arc, orogenic suits or I-type granites) to a pure sedimentary-material-dominated environment (S-type granites). We interpreted the magma source of the MMEs formed in an active environment (I-type granites). With the different degrees of mixing/mingling with granitic magma, the magma composition is getting closer and closer to the host granite (A-type granites). The biotite grains from granite crystallized in a transitional environment between A-type (field A) granites and S-type (field P) granites field. The geochemistry and geochronology results of Wangjiazhunag monzogranite has been reported by Wang J P et al. (2013) and Zhang et al. (2020), and they both concluded a typical affinity of A-type granites. These monzogranite has high alkali content, low CaO content and enrichment of Nb, Ga and Y. All of this features are consistent with classic A-type granite. In addition, they are all plotted in the field of A-type granites in the classification diagram of Na_2O vs. K_2O, (K_2O + Na_2O) vs. 10 000 Ga/Al and (K_2O + MgO) vs. 10 000 Ga/Al. Hence we interpreted the host rocks show an affinity of A-type granites.

On the chondrite-normalized REE distribution patterns, the MMEs show a strong negative Eu anomalies, enrichment in LREEs and relatively flat HREE patterns (Fig. 9a). On the primitive mantle-normalized spidergram (Fig. 9b), the MMEs have distinctly negative anomalies in Ba, K, Sr, P and Ti. The negative anomalies of Ba, K, Sr and Eu might be associated with residue of K-feldspar and plagioclase in the magma source, whereas the negative anomalies of P should be attributed to the residue of apatite. The MMEs and host granite have mutually consistent composition patterns, suggesting similar magma source. However, the range of variation in the composition of MMEs is larger. This may be due to the fact that the composition of the host granite has reached uniformity, while the composition of MMEs differs greatly due to the degree of mixing/mingling.

4.2 Magmatic Mixing/Mingling

The enclaves in granite are multi-genetic, can be the xenolith of surrounding rock, the cognate fragments of cumulate minerals or early formed crystals from the host magma and the product of incomplete mixing of magma with different properties. The genetic types of MMEs in granite have been debated for a long time, but the latest research shows that the mixed origin of magma is the most important and widely accepted genet-

ic model (Temizel et al., 2014; Weidendorfer et al., 2014; Zhao et al., 2010; Slaby and Martin, 2007; Zhang et al., 2007; Barbarin, 2005; Perugini et al., 2003).

The MMEs in Wangjiazhuang granite are interpreted as magmatic mixing. According to the petrography characteristics of the MMEs, reaction rims generally are formed by rapid magma quenching between the MMEs and host granite with distinct boundary between the MMEs and host granite. The MMEs show typical magmatic structure such as porphyritic texture, micrograined hypidiomorphic, equigranular texture. All these indicate that the MMEs are magmatic origin and then experienced underquenching and mixing/mingling with granite magma.

The major and trace element analysis was carried out for the MMEs, combined with the previous geochemical analysis of the Wangjiazhuang granite (Table 2), indicating that the contents of Fe, Mg, Ti and Ca in the MMEs are higher than that in the host granite, and the variation range is also obvious. The results (Table 2) from Wang et al. (2015) show that the Wangjiazhuang granite have slightly positive initial $\varepsilon_{Nd}(t)$ values (+0.12– +1.13), high contents of Si, K, and Rb/Sr ratios (1.80 to 3.21, average 2.54), low contents of Mg and Cr, indicating that Wangjiazhuang granite can't be derived from mantle-derived melts, but from crustal-derived melts. Wang et al. (2015) proposed age of the Wangjiazhuang granite is ca. 2.5 Ga, but the MMEs have not been dated. However, according to the petrography characteristics of the MMEs, both the MMEs and host magma should be the contemporaneous product of magmatism. Based on the mineral chemical characteristics of biotite, the Mg content of biotite in the MMEs decreases gradually with the increase of Fe, showing an obvious linear negative correlation (Fig. 4). The biotite in the MMEs in the Mg-(Al^{VI} + Fe^{3+} + Ti)-(Fe^{2+} + Mn) classification diagram (Fig. 5) fall in both ferrobiotite and siderophyllite, and its MF value (Table 1) is 0.42–0.95, with a wide range of variation. These characteristics indicate that the different degrees of material exchange between granite magma and enclave magma influenced the degree of mixing, leading to the composition of biotite crystallized in the MMEs has a wide range of variation, which corresponds to a deep to shallow series color of enclaves in different samples. Biotite in MMEs with a deeper color index has higher Mg content, and its composition is close to or within the crust-mantle mixing area (Fig. 5).

As described above, the injection of enclave magma into granitic magma should be a continuous process. In the early stage of granite magma evolution, mafic magma derived from the melting of the enriched mantle was injected into the granite magma chamber. Due to the disturbance of the mafic magma injection and the thermal convection of the granite magma, the enclave magma is broken into small magma clusters. The granitic magma has higher initial temperature, mafic magma is strongly mixed and/or mingled by the granitic magma and the composition of the mafic magma was greatly affected by the composition of the granite magma, resulting in the composition of the biotite crystallized in the enclave is similar to the biotite in the host granite, both rich in Fe and poor in Mg, and forming an enclave with a lighter color index. In the late stage of the evolution of granitic magma, the viscosity of granitic magma increased with a drop in temperature and has lower competence to be mixed/mingled, resulting in the gradually weakened degree of mixing/mingling between granitic magma and the enclave magma injecting into the granite magma, and the decreasingly affected composition of the enclave magma by the granite magma. Therefore, the biotite crystallized from the inclusions retains the original characteristics of relatively rich Mg. As the degree of mixing/mingling changes from strong to weak, various types of inclusions with gradually increasing color rates are formed.

5 CONCLUSIONS

The following conclusions are drawn from this study.

(1) The biotite in biotite monzogranite is rich in Fe and poor in Mg, which belongs to siderophyllite, indicating that its material source is mainly from crust source. The biotite in the MMEs is relatively rich in Mg, and shows various composition, including siderophyllite and ferrobiotite. Both biotite species are formed at low oxygen fugacity.

(2) The MMEs has undergone a crust-mantle mixing process and recorded the process of magma mixing/mingling with the Wangjiazhuang granite. The injection of mafic enclave magma into the granite magma is a continuous process. The degree of mixing/mingling between granitic and mafic magma gradually decreased as the evolution of granitic magma.

ACKNOWLEDGMENTS

This study was supported by the National Natural Science Foundation of China (No. 42072222), the Fundamental Research Funds for the Central Universities, China University of Geosciences, Wuhan (Nos. CUGL180406 and CUGCJ1707), the Chinese Ministry of Education Fund (No. BP0719022) and the Open Fund from the State Key Laboratory of Geological Processes and Mineral Resources, China University of Geosciences, Wuhan (No. GRMR201901), and Chinese Academy of Sciences (No. QYZDY-SSW-DQC017). We appreciate constructive comments from the editors and two anonymous reviewers that substantially improved the manuscript during the revisions. The final publication is available at Springer via https://doi.org/10.1007/s12583-020-1376-9.

REFERENCES CITED

Abdel-Rahman, A. F. M., 1994. Nature of Biotites from Alkaline, Calc-Alkaline, and Peraluminous Magmas. *Journal of Petrology*, 35(2): 525–541. https://doi.org/10.1093/petrology/35.2.525

Abdel-Rahman, A. F. M., 1996. Discussion on the Comment on Nature of Biotites in Alkaline, Calc-Alkaline and Peraluminous Magmas. *Journal of Petrology*, 37(5): 1031–1035. https://doi. org/10.1093/petrology/37.5.1031

Bai, J., Dai, F. Y., 1996. The Early Precambrian Crustal Evolution of China. *Journal of Southeast Asian Earth Sciences*, 13: 205–214. https://doi.org/10.1016/0743-9547(96)00027-x

Bai, J., Dai, F. Y., 1998. Archean Crust of China. In: Ma, X. Y., Bai, J., eds., Precambrian Crustal Evolution of China. Springer, Beijing. 15–86

Barbarin, B., 2005. Mafic Magmatic Enclaves and Mafic Rocks Associated with some Granitoids of the Central Sierra Nevada Batholith, California: Nature, Origin, and Relations with the Hosts. *Lithos*, 80(1–4): 155–177. https://doi.org/10.1016/j.lithos.2004.05.010

Burkhard, D. J. M., 1991. Temperature and Redox Path of Biotite-Bearing

Intrusives: A Method of Estimation Applied to S- and I-Type Granites from Australia. *Earth and Planetary Science Letters*, 104(1): 89–98. https://doi.org/10.1016/0012-821x(91)90240-i

Chen, Z. G., Zhu, K., Liu, J. X., et al., 2021. Early Paleoproterozoic Tectonic Evolution of Central Jiao-Liao-Ji Belt: Evidence from Muniuhe and Dafangshen Plutons. *Earth Science*, 46(5): 1710–1727. https://doi.org/10.3799/dqkx.2020.206 (in Chinese with English Abstract)

Deng, H., Kusky, T., Polat, A., et al., 2013. Geochemistry of Neoarchean Mafic Volcanic Rocks and Late Mafic Dikes in the Zanhuang Complex, Central Orogenic Belt, North China Craton: Implications for Geodynamic Setting. *Lithos*, 175/176: 193–212. https://doi.org/10.1016/j.lithos.2013.05.007

Deng, H., Kusky, T. M., Polat, A., et al., 2014. Geochronology, Mantle Source Composition and Geodynamic Constraints on the Origin of Neoarchean Mafic Dikes in the Zanhuang Complex, Central Orogenic Belt, North China Craton. *Lithos*, 205: 359 – 378. https://doi. org/10.1016/j.lithos.2014.07.011

Dong, Q., Du, Y. S., Cao, Y., et al., 2011. Compositional Characteristics of Biotites in Wushan Granodiorite, Jiangxi Province: Implications for Petrogenesis and Mineralization. *Mineralogy and Petrology*, 31(2): 1–6 (in Chinese with English Abstract)

Du, L. L., Yang, C. H., Song, H. X., et al., 2020. Neoarchean-Paleoproterozoic Multi-Stage Geological Events and Their Tectonic Implications in the Fuping Complex, North China Craton. *Earth Science*, 45(9): 3179–3195. https://doi.org/10.3799/dqkx.2020.240 (in Chinese with English Abstract)

Duan, R. H., Liu, C. H., Shi, J. R., 2020. Studies on Metamorphic Zircons of Granitic Gneisses and Amphibolites in the Dengkou and Shetai Areas of the Khondalite Belt of the North China Craton: More Constraints on Its Northern Boundary. *Earth Science*, 45(9): 3386–3402. https://doi.org/10.3799/dqkx.2020.080 (in Chinese with English Abstract)

El Sheshtawi, Y. A., Salem, A. K. A., Aly, M. M., 1993. The Geochemistry of Ferrous Biotite and Petrogenesis of Wadi-El-Sheikh Granitoid Rocks Southwestern Sinai, Egypt. *Journal of African Earth Sciences* (*and the Middle East*), 16(4): 489–498. https://doi.org/10.1016/0899-5362(93)90106-z

Foster, M. D., 1960. Interpretation of Composition of Trioctahedral Micas. *Geological Survey Professional Paper*, 354B: 1–49

Gao, P., Zhao, Z. F., Zheng, Y. F., 2016. Magma Mixing in Granite Petrogenesis: Insights from Biotite Inclusions in Quartz and Feldspar of Mesozoic Granites from South China. *Journal of Asian Earth Sciences*, 123: 142–161. https://doi.org/10.1016/j.jseaes.2016.04.003

Geng, Y. S., Shen, Q. H., Ren, L. D., 2010. Late Neoarchean to Early Paleoproterozoic Magmatic Events and Tectonothermal Systems in the North China Craton. *Acta Petrologica Sinica*, 26(7): 1945–1966 (in Chinese with English Abstract)

Geng, Y. S., Du, L. L., Ren, L. D., 2012. Growth and Reworking of the Early Precambrian Continental Crust in the North China Craton: Constraints from Zircon Hf Isotopes. *Gondwana Research*, 21(2/3): 517–529. https://doi.org/10.1016/j.gr.2011.07.006

Govindaraju, K., 1994. Compilation of Working Values and Sample Description for Geostandards. *Geostandards and Geoanalytical Research*, 18: 1–158. https://doi.org/10.1046/j.1365-2494.1998.53202081.x-i1

Guo, M. J., Qian, J. H., Yin, C. Q., et al., 2021. Metamorphic Evolution and Tectonic Implications of Garnet Amphibolite from Yunzhongshan Terrane in Central North China Craton. *Earth Science*, 46(11): 3892–3909. https://doi.org/10.3799/dqkx.2021.016 (in Chinese with English Abstract)

Han, C. M., Xiao, W. J., Su, B. X., et al., 2014. Neoarchean Algoma-Type Banded Iron Formations from Eastern Hebei, North China Craton: SHRIMP U-Pb Age, Origin and Tectonic Setting. *Precambrian Research*, 251: 212–231. https://doi.org/10.1016/j.precamres.2014.06.019

Jiang, K., Wang, J. P., Kusky, T. M., et al., 2020. Neoarchean Seafloor Hydrothermal Metamorphism of Basalts in the Zanhuang Ophiolitic Mélange, North China Craton. *Precambrian Research*, 347(B6): 105832. https://doi.org/10.1016/j.precamres.2020.105832

Jiang, S. Y., Zhao, K. D., Jiang, Y. H., et al., 2006. New Type of Tin Mineralization Related to Granite in South China: Evidence from Mineral Chemistry, Element and Isotope Geochemistry. *Acta Petrologica Sinica*, 22(10): 2509–2516 (in Chinese with English Abstract)

Jiang, S. Y., Li, L., Zhu, B., et al., 2008. Geochemical and Sr-Nd-Hf Isotopic Compositions of Granodiorite from the Wushan Copper Deposit, Jiangxi Province and Their Implications for Petrogenesis. *Acta Petrologica Sinica*, 24(8): 1679–1690 (in Chinese with English Abstract)

Kusky, T. M., Li, J. H., 2003. Paleoproterozoic Tectonic Evolution of the North China Craton. *Journal of Asian Earth Sciences*, 22(4): 383–397. https://doi.org/10.1016/S1367-9120(03)00071-3

Kusky, T. M., Polat, A., Windley, B. F., et al., 2016. Insights into the Tectonic Evolution of the North China Craton through Comparative Tectonic Analysis: A Record of Outward Growth of Precambrian Continents. *Earth-Science Reviews*, 162: 387 – 432. https://doi. org/10.1016/j.earscirev.2016.09.002

Kusky, T. M., Windley, B. F., Polat, A., 2018. Geological Evidence for the Operation of Plate Tectonics throughout the Archean: Records from Archean Paleo-Plate Boundaries. *Journal of Earth Science*, 29(6): 1291–1303. https://doi.org/10.1007/s12583-018-0999-6

Kwan, L. C. J., Zhao, G. C., Yin, C. Q., et al., 2016. Metamorphic *P-T* Path of Mafic Granulites from Eastern Hebei: Implications for the Neoarchean Tectonics of the Eastern Block, North China Craton. *Gondwana Research*, 37: 20–38. https://doi.org/10.1016/j.gr.2016.05.004

Li, T. S., Zhai, M. G., Peng, P., et al., 2010. Ca. 2.5 Billion Year Old Coeval Ultramafic-Mafic and Syenitic Dykes in Eastern Hebei: Implications for Cratonization of the North China Craton. *Precambrian Research*, 180(3/4): 143–155. https://doi.org/10.1016/j.precamres.2010.04.001

Li, L., Zhai, W. J., 2019. Geochemistry and Petrogenesis of the ca. 2.5 Ga High-K Granitoids in the Southern North China Craton. *Journal of Earth Science*, 30(3): 647–665. https://doi.org/10.1007/s12583-019-0895-8

Lin, W. W., Peng, L. J., 1994. The Estimation of Fe^{3+} and Fe^{2+} Contents in Amphibole and Biotite from EMPA Data. *Journal of Changchun University of Earth Sciences*, 24(2): 155–162 (in Chinese with English Abstract)

Lü, Z. C., Duan, G. Z., Dong, G. H., 2003. Mineral Chemistry of Biotite from Granites Associated with Different Mineralization in Three Stages of Yanshanina Period in the Southern-Middle Parts of the Da Hinggan Ling Mountains and Its Petrogenetic and Metallogenic Significance. *Acta Mineralogica Sinica*, 23(2): 177–184. https://doi.org/10.16461/j.cnki.1000-4734.2003.02.015 (in Chinese with English Abstract)

Liu, Y. S., Hu, Z. C., Gao, S., et al., 2008. *In situ* Analysis of Major and Trace Elements of Anhydrous Minerals by LA-ICP-MS without Applying an Internal Standard. *Chemical Geology*, 257(1/2): 34–43. https://doi.org/10.1016/j.chemgeo.2008.08.004

Liu, L., Qiu, J. S., Li, Z., 2013. Origin of Mafic Microgranular Enclaves (MMEs) and Their Host Quartz Monzonites from the Muchen Pluton in Zhejiang Province, Southeast China: Implications for Magma Mixing and Crust-Mantle Interaction. *Lithos*, 160(1): 145–163. https://doi.org/10.1016/j.lithos.2012.12.005

Ma, C. Q., Yang, K. G., Tang, Z. H., et al., 1994. Magma-Dynamics Granitoids: Theory, Methods and a Case Study of the Eastern Hubei Granitoids. China University of Geosciences Press, Wuhan. 210–212 (in Chinese)

Ma, Q., Zheng, J. P., Griffin, W. L., et al., 2012. Triassic "Adakitic" Rocks in an Extensional Setting (North China): Melts from the Cratonic Lower Crust. *Lithos*, 149: 159–173. https://doi. org/10.1016/j. lithos. 2012. 04.017

Ma, X. D., Guo, J. H., Liu, F., et al., 2013. Zircon U-Pb Ages, Trace Elements and Nd-Hf Isotopic Geochemistry of Guyang Sanukitoids and Related Rocks: Implications for the Archean Crustal Evolution of the Yinshan Block, North China Craton. *Precambrian Research*, 230: 61–78. https://doi.org/10.1016/j.precamres.2013.02.001

Ma, S. T., Li, X. P., Liu, H., et al., 2019. Ultrahigh Temperature Metamorphic Record of Pelitic Granulites in the Huangtuyao Area of the Huai'an Complex, North China Craton. *Journal of Earth Science*, 30(6): 1178–1196. https://doi.org/10.1007/s12583-019-1245-6

McDonough, W., Sun, S. S., 1995. The Composition of the Earth. *Chemical Geology*, 120(3/4): 223–253. https://doi. org/10.1016/0009-2541(94) 00140-4

Ning, W. B., Wang, J. P., Xiao, D., et al., 2019. Electron Probe Microanalysis of Monazite and Its Applications to U-Th-Pb Dating of Geological Samples. *Journal of Earth Science*, 30(5): 952–963. https:// doi.org/10.1007/s12583-019-1020-8

Nutman, A. P., Wan, Y. S., Du, L. L., et al., 2011. Multistage Late Neoarchaean Crustal Evolution of the North China Craton, Eastern Hebei. *Precambrian Research*, 189(1/2): 43 – 65. https://doi. org/ 10.1016/j.precamres.2011.04.005

Peng, H. M., 1997. Geological Characteristics of Biotite from Yangxi Granite Body and Their Geological Implications. *Acta Petrrologica et Mineralogica*, 16(3): 271–281 (in Chinese with English Abstract)

Peng, T. P., Wilde, S. A., Fan, W. M., et al., 2013. Late Neoarchean Potassic High Ba-Sr Granites in the Taishan Granite-Greenstone Terrane: Petrogenesis and Implications for Continental Crustal Evolution. *Chemical Geology*, 344: 23–41. https://doi. org/10.1016/j. chemgeo. 2013.02.012

Perugini, D., Poli, G., Christofides, G., et al., 2003. Magma Mixing in the Sithonia Plutonic Complex, Greece: Evidence from Mafic Microgranular Enclaves. *Mineralogy and Petrology*, 78(3): 173–200. https://doi.org/10.1007/s00710-002-0225-0

Pignatelli, I., Faure, F., Mosser-Ruck, R., 2016. Self-Mixing Magma in the Ruiz Peak Rhyodacite (New Mexico, USA): A Mechanism Explaining the Formation of Long Period Polytypes of Mica. *Lithos*, 266/267: 332–347. https://doi.org/10.1016/j.lithos.2016.10.024

Rieder, M., Cavazzini, G., D'yakonov, Y. S., et al., 1999. Nomenclature of the Micas. *Mineralogical Magazine*, 63(2): 267–279. https://doi. org/ 10.1180/minmag.1999.063.2.13

Shabani, A. A. T., Lalonde, A. E., Whalen, J. B., 2003. Composition of Biotite from Granitic Rocks of the Canadian Appalachian Orogen: A Potential Tectonomagmatic Indicator? *The Canadian Mineralogist*, 41(6): 1381–1396. https://doi.org/10.2113/gscanmin.41.6.1381

Slaby, E., Martin, H., 2007. Mafic and Felsic Magma Interaction in Granites: The Hercynian Karkonosze Pluton (Sudetes, Bohemian Massif). *Journal of Petrology*, 49(2): 353–391. https://doi.org/10.1093/ petrology/egm085

Speer, J. A., 1987. Evolution of Magmatic AFM Mineral Assemblages in Granitoid Rocks: The Hornblende + Melt = Biotite Reaction in the Liberty Hill Pluton, South Carolina. *American Mineralogist*, 72(9/10): 863–878

Stone, D., 2000. Temperature and Pressure Variations in Suites of Archean Felsic Plutonic Rocks, Berens River Area, Northwest Superior Province, Ontario, Canada. *The Canadian Mineralogist*, 38(2): 455–470. https://doi.org/10.2113/gscanmin.38.2.455

Sun, S. H., Yu, J., 1989. Interpretation of Chemical Composition and Subdivision of Mg-Fe Micas, Part B: The Natural Subdivision of Mg-Fe Micas. *Scientia Geologica Sinica*, 2: 176–189 (in Chinese with English Abstract)

Temizel, İ., Arslan, M., Abdioğlu, E., et al., 2014. Mineral Chemistry and Thermobarometry of Eocene Monzogabbroic Stocks from the Bafra (Samsun) Area in Turkey: Implications for Disequilibrium Crystallization and Emplacement Conditions. *International Geology Review*, 56(10): 1226–1245. https://doi.org/10.1080/00206814.2014.933363

Trap, P., Faure, M., Monié, P., et al., 2009a. The Zanhuang Massif, the Second and Eastern Suture Zone of the Paleoproterozoic Trans-North China Orogen. *Precambrian Research*, 172(1): 80–98. https://doi.org/ 10.1016/j.precamres.2009.03.011

Trap, P., Faure, M., Lin, W., et al., 2009b. The Luliang Massif: A Key Area for the Understanding of the Palaeoproterozoic Trans-North China Belt, North China Craton. *Journal of the Geological Society*, *London*, *Special Publications*, 33: 99–125. https://doi.org/10.1144/sp323.5

Trap, P., Faure, M., Augier, R., et al., 2011. Syn-Collisional Channel Flow and Exhumation of Paleoproterozoic High Pressure Rocks in the Trans-North China Orogen: The Critical Role of Partial-Melting and Orogenic Bending. *Gondwana Research*, 20(2/3): 498–515. https://doi. org/10.1016/j.gr.2011.02.013

Wang, J. P., Kusky, T. M., Polat, A., et al., 2013. A Late Archean Tectonic Mélange in the Central Orogenic Belt, North China Craton. *Tectonophysics*, 608: 929–946. https://doi.org/10.1016/j.tecto.2013.07.025

Wang, J. P., Kusky, T. M., Wang, L., et al., 2015. A Neoarchean Subduction Polarity Reversal Event in the North China Craton. *Lithos*, 220–223: 133–146. https://doi.org/10.1016/j.lithos.2015.01.029

Wang, J. P., Deng, H., Kusky, T. M., et al., 2017a. Comments to "Paleoproterozoic Meta-Carbonates from the Central Segment of the Trans-North China Orogen: Zircon U-Pb Geochronology, Geochemistry, and Carbon and Oxygen Isotopes" by Tang et al., 2016, *Precambrian Research*, 284: 14–29. *Precambrian Research*, 294: 344–349. https://doi.org/10.1016/j.precamres.2017.01.021

Wang, J. P., Kusky, T. M., Wang, L., et al., 2017b. Structural Relationships along a Neoarchean Arc-Continent Collision Zone, North China Craton. *Geological Society of America Bulletin*, 129(1/2): 59–75. https://doi.org/ 10.1130/b31479.1

Wang, J. P., Kusky, T. M., Wang, L., et al., 2017c. Petrogenesis and Geochemistry of circa 2.5 Ga Granitoids in the Zanhuang Massif: Implications for Magmatic Source and Neoarchean Metamorphism of the North China Craton. *Lithos*, 268–271: 149–162. https://doi. org/ 10.1016/j.lithos.2016.10.028

Wang, J. P., Li, X. W., Ning, W. B., et al., 2019. Geology of a Neoarchean Suture: Evidence from the Zunhua Ophiolitic Mélange of the Eastern Hebei Province, North China Craton. *GSA Bulletin*, 131(11/12): 1943–1964. https://doi.org/10.1130/b35138.1

Wang, W., Liu, S. W., Santosh, M., et al., 2013. Zircon U-Pb-Hf Isotopes and Whole-Rock Geochemistry of Granitoid Gneisses in the Jianping Gneissic Terrane, Western Liaoning Province: Constraints on the Neoarchean Crustal Evolution of the North China Craton. *Precambrian Research*, 224: 184–221. https://doi. org/10.1016/j. precamres. 2012. 09.019

Weidendorfer, D., Mattsson, H. B., Ulmer, P., 2014. Dynamics of Magma Mixing in Partially Crystallized Magma Chambers: Textural and Petrological Constraints from the Basal Complex of the Austurhorn Intrusion (SE Iceland). *Journal of Petrology*, 55(9): 1865–1903. https://doi.org/10.1093/petrology/egu044

Wilde, S. A., Cawood, P. A., Wang, K. Y., et al., 2005. Granitoid Evolution in the Late Archean Wutai Complex, North China Craton. *Journal of Asian Earth Sciences*, 24(5): 597–613. https://doi.org/10.1016/j.jseaes.2003.11.006

Wones, D. R., Eugster, H. P., 1965. Stability of Biotite: Experiment, Theory, and Application. *The American Mineralogist*, 50: 1228–1272

Wu, C. M., Zhao, G. C., 2006. The Applicability of the GRIPS Geobarometry in Metapelitic Assemblages. *Journal of Metamorphic Geology*, 24(4): 297–307. https://doi.org/10.1111/j.1525-1314.2006. 00638.x

Wu, C. M., Zhao, G. C., 2007. The Metapelitic Garnet-Biotite-Muscovite-Aluminosilicate-Quartz (GBMAQ) Geobarometer. *Lithos*, 3/4(97): 365–372. https://doi.org/10.1016/j.lithos.2007.01.003

Wu, C. M., 2020. Calibration of the Biotite-Muscovite Geobarometer for Metapelitic Assemblages Devoid of Garnet or Plagioclase. *Lithos*, 372: 105668. https://doi.org/10.1016/j.lithos.2020.105668

Wu, M. L., Zhao, G. C., Sun, M., et al., 2014. Tectonic Affinity and Reworking of the Archaean Jiaodong Terrane in the Eastern Block of the North China Craton: Evidence from LA-ICP-MS U-Pb Zircon Ages. *Geological Magazine*, 151(2): 365–371. https://doi.org/10.1017/s0016756813000721

Xie, Y. W., Zhang, Y. Q., 1987. Typomorphic Peculiarities of Biotites from Different Genetic Types of Granite in the Hengduanshan Region. *Acta Mineralogica Sinica*, 7(3): 245 – 254. https://doi. org/10.16461/j. cnki. 1000-4734.1987.03.007 (in Chinese with English Abstract)

Xu, B., Jiang, S. Y., Wang, R., et al., 2015. Late Cretaceous Granites from the Giant Dulong Sn-Polymetallic Ore District in Yunnan Province, South China: Geochronology, Geochemistry, Mineral Chemistry and Nd-Hf Isotopic Compositions. *Lithos*, 218/219: 54–72. https://doi.org/10.1016/j.lithos.2015.01.004

Xu, Y. M., Jiang, S. Y., Zhu, Z. Y., et al., 2013. Geochronology, Geochemistry and Mineralogy of Ore-Bearing and Ore-Barren Intermediate-Acid Intrusive Rocks from the Jiurui Ore District, Jiangxi Province and Their Geological Implications. *Acta Petrologica Sinica*, 29(12): 4291–4310 (in Chinese with English Abstract)

Yang, S. Y., Jiang, S. Y., 2013. Occurrence and Significance of a Quartz-Amphibole Schist Xenolith within a Mafic Microgranular Enclave in the Xiangshan Volcanic-Intrusive Complex, SE China. *International Geology Review*, 55(7): 894 – 903. https://doi. org/10.1080/00206814.2012.752662

Zhai, M. G., Santosh, M., 2011. The Early Precambrian Odyssey of the North China Craton: A Synoptic Overview. *Gondwana Research*, 20(1): 6–25. https://doi.org/10.1016/j.gr.2011.02.005

Zhang, F., Wang, Y. B., Du, L. L., et al., 2020. Zircon U-Pb Ages and Geochemistry of the Late Archaean Granitoids in the Zanhuang Complex: Records of an Arc-Continent Collision Event at the End of Archaean. *Geological Journal*, 55(2): 1391–1408. https://doi.org/10.1002/gj.3500

Zhang, J., Zhang, H. F., Lu, X. X., 2013. Zircon U-Pb Age and Lu-Hf Isotope Constraints on Precambrian Evolution of Continental Crust in the Songshan Area, the South-Central North China Craton. *Precambrian Research*, 226: 1–20. https://doi.org/10.1016/j.precamres.2012.11.015

Zhang, Q. C., Pan, G. Q., Li, C. D., et al., 2007. Granitic Magma Mixing versus Basaltic Magma Mixing: New Viewpoints on Granitic Magma Mixing Process: Some Crucial Questions on Granite Study. *Acta Petrologica Sinica*, 23(5): 1141–1152 (in Chinese with English Abstract)

Zhang, Z. Z., Gu, L. X., Wu, C. Z., et al., 2005. Weiya Complex, Estern Tianshan: Single-Sourced or Diverse-Sourced? —Evidence from Biotite. *Geochimica*, 34(4): 328–338 (in Chinese with English Abstract)

Zhao, G. C., 2009. Metamorphic Evolution of Major Tectonic Units in the Basement of the North China Craton: Key Issues and Discussion. *Acta Petrologica Sinica*, 25(8): 1772 – 1792 (in Chinese with English Abstract)

Zhao, G. C., Wilde, S. A., Cawood, P. A., et al., 1999. Thermal Evolution of Two Textural Types of Mafic Granulites in the North China Craton: Evidence for both Mantle Plume and Collisional Tectonics. *Geological Magazine*, 136(3): 223–240. https://doi.org/10.1017/s001675689900254x

Zhao, G. C., Wilde, S. A., Cawood, P. A., et al., 2001. Archean Blocks and Their Boundaries in the North China Craton: Lithological, Geochemical, Structural and *P-T* Path Constraints and Tectonic Evolution. *Precambrian Research*, 107(1/2): 45 – 73. https://doi. org/10.1016/s0301-9268(00)00154-6

Zhao, G. C., Zhai, M. G., 2013. Lithotectonic Elements of Precambrian Basement in the North China Craton: Review and Tectonic Implications. *Gondwana Research*, 23(4): 1207 – 1240. https://doi.org/10.1016/j.gr.2012.08.016

Zhao, K. D., Jiang, S. Y., Jiang, Y. H., et al., 2005. Mineral Chemistry of the Qitianling Granitoid and the Furong Tin Ore Deposit in Hunan Province, South China: Implication for the Genesis of Granite and Related Tin Mineralization. *European Journal of Mineralogy*, 17(4): 635–648. https://doi.org/10.1127/0935-1221/2005/0017-0635

Zhao, K. D., Jiang, S. Y., Zhu, J. C., et al., 2010. Hf Isotopic Composition of Zircons from the Huashan-Guposhan Intrusive Complex and Their Mafic Enclaves in Northeastern Guangxi: Implication for Petrogenesis. *Chinese Science Bulletin*, 55(6): 509 – 519. https://doi. org/10.1007/s11434-009-0314-0

Zhao, K. D., Liu, G. Q., Jiang, S. Y., 2019. Petrogenesis and Tectonic Implications of the Yuhuashan A-Type Volcanic-Intrusive Complex and Mafic Microgranular Enclaves in the Gan-Hang Volcanic Belt, Southeast China. *Journal of Geology*, 127(1): 37 – 59. https://doi. org/10.1086/700408

Zhao, M., Yang, S. Y., Zuo, R. G., et al., 2015. Magmatic Evolution Characteristics of Xiangshan Volcanic-Intrusive Complex from the Gan-Hang Belt: Studies on the Mineral Chemistry of Plagioclase and Biotite. *Acta Petrologica Sinica*, 31(3): 759 – 768 (in Chinese with English Abstract)

Zhong, Y. T., He, C., Chen, N. S., et al., 2018. Tectonothermal Records in Migmatite-Like Rocks of the Guandi Complex in Zhoukoudian, Beijing: Implications for Late Neoarchean to Proterozoic Tectonics of the North China Craton. *Journal of Earth Science*, 29(5): 1254 – 1275. https://doi.org/10.1007/s12583-018-0856-7

Zhou, Z. X., 1988. Chemical Characteristics of Mafic Mica in Intrusive Rocks and Its Geological Meaning. *Acta Petrologica Sinica*, 4(3): 63–73 (in Chinese with English Abstract)

Zhu, Z. Y., Jiang, S. Y., Hu, J., et al., 2014. Geochronology, Geochemistry, and Mineralization of the Granodiorite Porphyry Hosting the Matou Cu-Mo (±W) Deposit, Lower Yangtze River Metallogenic Belt, Eastern China. *Journal of Asian Earth Sciences*, 79: 623–640. https://doi.org/10.1016/j.jseaes.2013.07.033